Hindawi
Shock and Vibration
Volume 2023, Article ID 5491832, 12 pages
https://doi.org/10.1155/2023/5491832

Research Article

Study on the Seismic Response and Aseismic Measure of Fault-Crossing Tunnels under Combined Action of Fault Dislocation and Seismic Motions

Jieli Li,[1] **Zhiguo Ma**,[1] **Ruohan Li**,[2] **Zhensheng Cao**,[1] **and Shaoqiang Zhang**[1]

[1]*Powerchina Roadbridge Group Co., Ltd, Beijing 100048, China*
[2]*Department of Geotechnical Engineering, Tongji University, 1239 Siping Road, Shanghai 200092, China*

Correspondence should be addressed to Ruohan Li; lirh@tongji.edu.cn

Received 11 September 2022; Revised 4 December 2022; Accepted 19 April 2023; Published 30 April 2023

Academic Editor: Guangjian Liu

Seismic investigation revealed that a fault fracture zone is one of the most vulnerable areas of mountain tunnels in earthquakes. For the tunnel crossing secondary fault, the fault may be permanently dislocated by the causative faults during earthquakes, making the tunnel subject to combined action of seismic motion and fault dislocation, which makes the seismic response of the tunnel more complicated. In order to investigate the seismic response of fault-crossing tunnels in this case and explore the suitability of different aseismic measures, three-dimensional numerical models with different widths of faults and different aseismic measures were developed in this study. By inputting accelerogram considering permanent displacements, the seismic responses of fault-crossing tunnels under the combined action of seismic motion and fault dislocation were simulated. The results showed that the acceleration and stress of the tunnel-crossing narrow fault are larger than those crossing wide faults during earthquakes. Grouting reinforcement can reduce the acceleration and stress of the tunnel within the fault during earthquakes, while flexible joints will increase the acceleration of the tunnel within the fault and increase the stress of the tunnel-crossing wide fault. For fault-crossing tunnels, if the fault width is narrow than the tunnel diameter, the best aseismic measure installs grouting reinforcement and flexible joints; if the fault width is wider than 10 times of the tunnel diameter, the best aseismic measure installs grouting reinforcement.

1. Introduction

With the rapid growth of infrastructure demand, the rate of highway and railroad tunnel construction has increased by leaps and bounds, which has led to more complex geological conditions that tunnel construction can meet with. Tunnel damages in recent years have challenged the traditional idea that mountain tunnels have good seismic performance [1–4], which has prompted many scholars and engineers to study the seismic response and improve the seismic design of tunnels and other underground structures.

Earthquake damage investigations have shown that a fault fracture zone is one of the most dangerous areas for mountain tunnels [5–7]. Therefore, several studies on the seismic response of fault-crossing tunnels using model tests [8–10] and numerical simulations [11–13] have been carried out. When a fault dislocates, the tunnel will subject to severe damage due to the intense shear action [10, 14]. If the fault is not dislocated, the difference in the longitudinal mechanical properties of the strata will also cause uneven deformation in the longitudinal direction of the tunnel [7, 15]. The reflection and refraction of seismic waves on the fault interface also have negative effects on tunnel deformation [16, 17]. In the

case of tunnels crossing secondary faults, faults may be permanently dislocated by causative faults during earthquakes and tunnels will suffer from the combined action of fault dislocation and seismic motions. Due to the complex interaction of the fault-rock-tunnel system, the understanding of the seismic response mechanism of fault-crossing tunnels is not yet complete, and there is no consensus on the best aseismic measure, which leads to engineering practice lagging behind research.

In order to mitigate the damage of fault-crossing tunnels, several aseismic measures have been proposed: flexible joints can reduce the deformation of the tunnel by concentrating the permanent deformation of the fault to the joints through their own deformation [18, 19]. Buffer layers can reduce the transfer of earthquake energy to the tunnel by absorbing the deformation of the ground and thus reduce the damage of the tunnel [20, 21]. Fiber concrete can reduce the tunnel damage by enhancing the mechanical properties of the tunnel [21, 22]. Grouting reinforcement can reduce the tunnel damage by enhancing the mechanical properties of the strata in a certain range outside the tunnel and reducing the deformation of the strata within the fault [23]. However, few studies have been conducted to compare the seismic mitigation effects of different aseismic measures and evaluate the suitability of different aseismic measures. At the same time, few studies have been carried out to investigate the seismic response of tunnels crossing secondary faults, which may suffer from the combined action of seismic motions and fault dislocation during earthquakes.

In this paper, three-dimensional numerical models were developed for tunnels crossing secondary faults and the seismic response of tunnels crossing different widths of faults is investigated. Two aseismic measures, grouting reinforcement and flexible joints, were compared in terms of their aseismic effects in tunnels crossing different widths of faults. The present study can provide references and suggestions for the seismic design of tunnels across faults.

2. Numerical Model

2.1. Model Setup. Nonlinear finite element numerical models were established in ABAQUS to simulate the seismic response of the fault-crossing tunnel and verify the aseismic effect of different aseismic measures. Figure 1 shows the 3D model with a fault dip angle of 60° and fault widths of 10 m and 100 m, respectively. The diameter of the tunnel is 9.5 m, and the burial depth is 20 m. For the model with flexible joints, flexible joints with a width of 0.5 m are set at 6 m intervals in the lining of the fault. For the model with grouting zones, the strata within 0.5 times the diameter of the tunnel on the outside of the inner lining of the fault were set as grouting zones. The details of the two damping measures are shown in Figure 1.

In the numerical simulation, the tunnel lining is tied with the surrounding rock, and it is assumed that there is no relative slipping between lining and surrounding rock. Frictional contact between the fault and surrounding rock is used, and the friction coefficient is set to be 0.4. The Mohr–Coulomb criterion is used to simulate the elasto-plastic behavior of the surrounding rock, fault, and grouting zone, and tunnel lining and flexible joints are assumed to be linear elastic. The model material parameters are shown in Table 1. Rayleigh damping is adopted in the simulation, and the damping ratio is set to be 0.05. The first two modes of the numerical model were selected to construct the damping matrix. To simulate the shear deformation of the ground under the action of shear waves, the equal displacement boundary is set on the lateral side of the model, so that the nodes at the same height move simultaneously. The synthetic wave, Wenchuan wave, and Kobe wave were used in the simulation as input seismic motions, as shown in Figure 2, and the peak ground acceleration is 0.3 g, which corresponds to a peak acceleration of 10% of the exceedance probability in 50 years.

2.2. Ground Motion Input. Fault-crossing tunnels may suffer from the combined action of fault displacement and ground motions under strong earthquakes. While the causes of permanent displacement of secondary faults are complex, some scholars believe that rupture occurs under the perturbation of earthquakes due to the initial stress level within the fault close to the material strength [24]. It is difficult to realistically reproduce the complex stress conditions and rupture processes within the fault in numerical simulations, so this paper implements the simulation of the permanent displacement of the fault by applying ground motion considering the permanent displacement on both sides of the fault.

The permanent displacement of a fault should be generated and ended at a certain moment of earthquake occurrence. Chao et al. [25] proposed the energy distribution ratio to determine the beginning and the end of the fault displacement and concluded that the fault movement starts when the energy distribution ratio reaches 25% and ends when the energy distribution ratio reaches 65%.

The detailed description of the seismic wave construction process is as follows: the synthetic wave energy time history is plotted in Figure 3, and it can be found that the seismic wave energy reaches 25% at 3.5 s and 65% at 6.5 s, so the start and end moments of the permanent displacement of the fault are set to be 3.5 s and 6.5 s. The displacement time history is obtained by integrating the synthetic wave acceleration and increasing the displacement linearly by a total of 0.1 m between 3.5 s and 6.5 s. The displacement time history after adding the permanent displacement is obtained, as shown in Figure 4. The acceleration time history considering the permanent displacement can be obtained by deriving the displacement time curve, as shown in Figure 5. A slip fracture surface is set in the center of the fault, and the original synthetic wave and the synthetic wave considering the permanent displacement are applied on both sides of the slip fracture surface to achieve the combined action of fault displacement and ground motions.

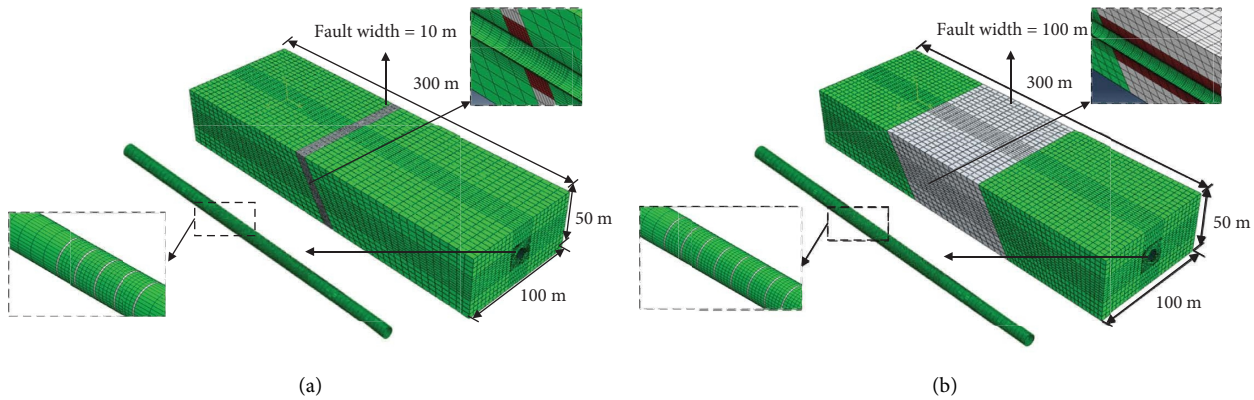

Figure 1: Diagram of models: (a) model with a 10 m fault and (b) model with a 100 m fault.

Table 1: Mechanical properties.

	Elastic modulus (MPa)	Density (kg/m^3)	Poisson's ratio	Cohesion (kPa)	Friction angle (°)
Surrounding rock	6000	2300	0.30	700	39
Fault	300	1700	0.35	100	20
Lining	30000	2500	0.2	—	—
Grouting zone	6000	2200	0.30	900	35
Flexible joint	600	2100	0.35	150	25

2.3. Analysis Procedures. In order to analyze the seismic response of tunnels crossing different widths of faults and explore the suitability of different seismic mitigation measures, eight numerical models were established, as shown in Table 2. The models with fault widths of 10 m and 100 m are used to compare the effect of the fault width on tunnel response under the combined action of fault dislocation and ground motions. In addition, three types of aseismic measures, namely, grouting, flexible joint, and grouting reinforcement + flexible joint, are installed in the models with different fault widths to verify the suitability of various damping measures; the details of these aseismic measures are plotted in Figure 6.

3. Results

3.1. Tunnel Responses with Different Fault Widths. The final deformation of the tunnel in the calculated conditions for the fault widths of 10 m and 100 m is plotted in Figure 7. It can be found that the final deformation of the tunnel is consistent with stratigraphic deformation, with a permanent deformation of 0.1 m, between the tunnels on both sides of the fault. Although a slip fracture surface is set in the center of the fault, tunnel deformation is not concentrated near the slip fracture surface but is evenly distributed over the fault width.

The peak acceleration of the tunnel vault along the longitudinal direction of the two models without aseismic measures is plotted in Figure 8, which indicates that the acceleration of the tunnel inside the fault is significantly greater than that of the tunnel in the surrounding rock on both sides of the fault. In addition, for tunnels located within a certain range on both sides of the fault, the acceleration of tunnels located at the hanging wall is greater than that located at the footwall, and this phenomenon is particularly significant when the fault width is small, which is also consistent with the upper plate effect observed in the seismic investigation [6]. For a fault with a width of 100 m, peak tunnel acceleration appears along the longitudinal direction with two peaks located near the two interfaces of the fault. This is because seismic waves incident vertically from the bottom are reflected through the fault intersections and superimposed with the incident waves at this location, which increases the acceleration there. For the fault with a width of 10 m, the two peaks overlap due to the small width of the fault, making the peak acceleration of the tunnel within the fault exceed the peak acceleration of the tunnel within the fault with a width of 100 m.

The maximum and minimum principal stresses in the tunnel for the two cases without aseismic measures are plotted in Figure 9. For the model with a 10 m fault, the maximum principal stress of the tunnel is 111.1 MPa and the minimum principal stress is 70.1 MPa in the synthetic wave case; the maximum principal stress of the tunnel is 107.8 MPa and the minimum principal stress is 94.0 MPa in the Wenchuan wave case; the maximum principal stress of the tunnel is 106.8 MPa and the minimum principal stress is 88.3 MPa in the Kobe wave case. For the model with a 100 m fault, the maximum principal stress of the tunnel is 46.5 MPa and the minimum principal stress is 42.7 MPa in the synthetic wave case; the maximum principal stress of the tunnel is 32.8 MPa and the minimum principal stress is 40.0 MPa in

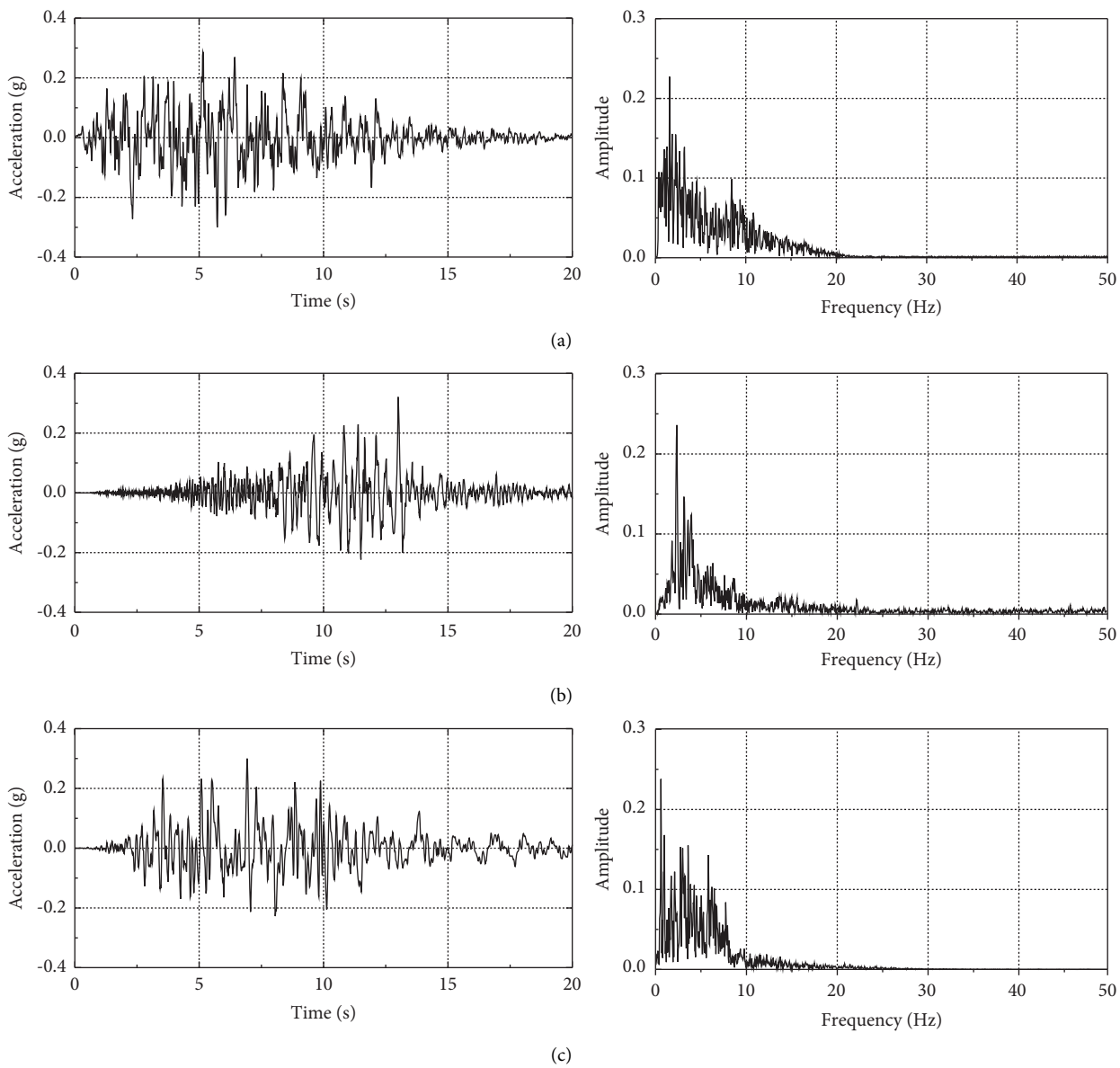

Figure 2: Accelerograms and Fourier spectra of seismic motions: (a) synthetic wave; (b) Wenchuan wave; (c) Kobe wave.

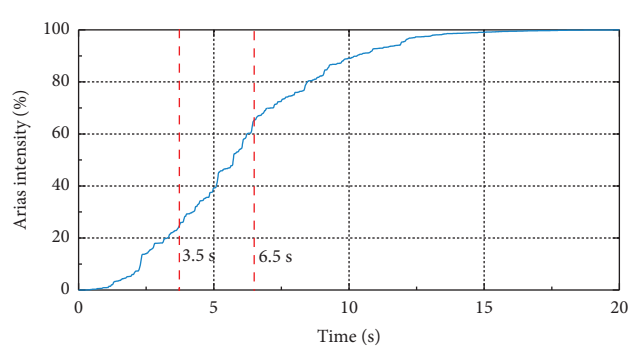

Figure 3: Energy time history of synthetic waves.

the Wenchuan wave case; the maximum principal stress of the tunnel is 33.1 MPa and the minimum principal stress is 28.9 MPa in the Kobe wave case. Different from the seismic response of fault-crossing tunnels only considering the seismic motions [26], the stress of the tunnel in narrow faults is greater than that in wide faults. This is because that the

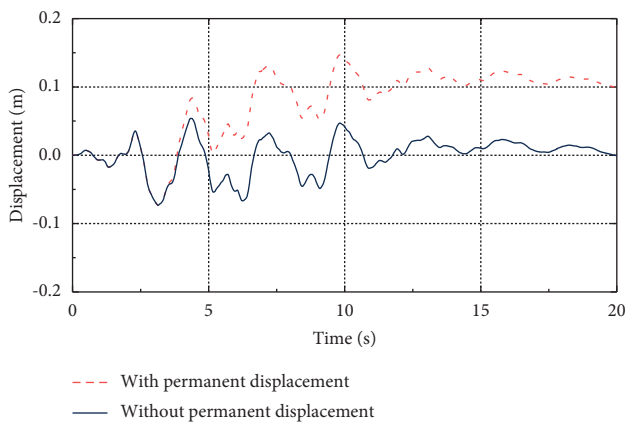

Figure 4: Displacement time history of synthetic waves.

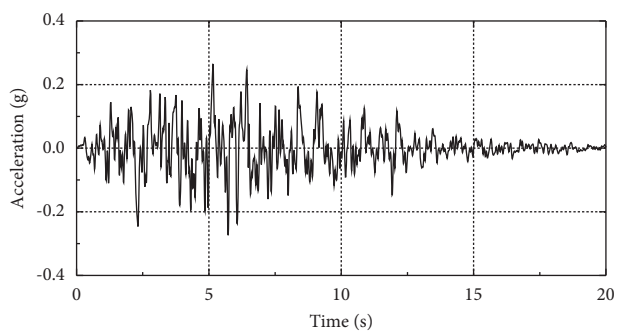

Figure 5: Accelerogram of synthetic wave contains permanent displacement.

Table 2: Analysis cases.

Cases	Fault width (m)	Aseismic measure
1	10	None
2	10	Flexible joint
3	10	Grouting
4	10	Flexible joint + grouting
5	100	None
6	100	Flexible joint
7	100	Grouting
8	100	Flexible joint + grouting

same permanent displacement in narrow faults will produce greater relative deformation in the tunnel, as shown in Figure 7, which also indicates that the response of the fault-crossing tunnel is to some extent dominant by the permanent displacement of the fault.

3.2. Aseismic Effect of Different Aseismic Measures. The distribution of the peak acceleration of the tunnel in a 10 m fault is plotted in Figure 10. It can be seen that the installation of different aseismic measures has little effect on tunnel acceleration and does not change the distribution of tunnel acceleration. In the synthetic wave case, the peak tunnel acceleration in the fault is reduced from 8.88 m/s^2 to 8.52 m/s^2 by both grouting and grouting + flexible joints, while peak tunnel acceleration is slightly increased to 8.97 m/s^2 by flexible joints. In the Wenchuan wave case, peak tunnel acceleration in the fault is reduced from 8.83 m/s^2 to 8.37 m/s^2 by both grouting and grouting + flexible joints, while peak tunnel acceleration is slightly increased to 9.00 m/s^2 by flexible joints. In the Kobe wave case, peak tunnel acceleration in the fault is reduced from 8.44 m/s^2 to 8.06 m/s^2 by both grouting and grouting + flexible joints, while peak tunnel acceleration is slightly increased to 8.58 m/s^2 by flexible joints.

The distribution of the peak acceleration of the tunnel in a 100 m fault is plotted in Figure 11. It can be seen that the installation of grouting significantly changes the distribution of tunnel acceleration within the fault. For three cases, the maximum acceleration within the fault is reduced from 8.31 m/s^2 to 7.91 m/s^2, 7.50 m/s^2 to 6.67 m/s^2, and 7.61 m/s^2 to 7.11 m/s^2, respectively. The installation of flexible joints does not change the acceleration distribution pattern of the tunnel but increases the maximum acceleration of the tunnel to 8.67 m/s^2, 8.08 m/s^2, and 8.34 m/s^2, respectively.

The maximum and minimum principal stresses in the model with a fault width of 10 m are plotted in Figure 12. It can be found that the installation of different aseismic measures does not change the distribution pattern of the principal stresses of the tunnel: the peak principal stresses are mainly concentrated at the interface between the fault and footwall. In the synthetic wave case, grouting reduces the maximum principal stress to 69.8 MPa and the minimum principal stress to 48.8 MPa; flexible joints reduce the maximum principal stress to 76.9 MPa and the minimum principal stress to 65.5 MPa; for the model with both aseismic measures installed, the maximum principal stress is reduced to 48.0 MPa and the minimum principal stress is reduced to 42.6 MPa. In the Wenchuan wave case, grouting reduces the maximum principal stress to 67.3 MPa and the minimum principal stress to 67.3 MPa; flexible joints increase the maximum principal stress to 122.4 MPa and the minimum principal stress to 103.2 MPa; for the model with both aseismic measures installed, the maximum principal stress is reduced to 86.9 MPa and the minimum principal stress is reduced to 73.1 MPa. In the Kobe wave case, grouting reduces the maximum principal stress to 66.3 MPa and the minimum principal stress to 66.4 MPa; flexible joints increase the maximum principal stress to 121.1 MPa and the minimum principal stress to 102.4 MPa; for the model with both aseismic measures installed, the maximum principal stress is reduced to 86.3 MPa and the minimum principal stress is reduced to 72.2 MPa.

The maximum and minimum principal stresses in the model with a fault width of 100 m are plotted in Figure 13. It can be found that the installation of grouting does not change the distribution pattern of principal stresses in the tunnel, and the peak maximum principal stresses are mainly concentrated at the interface between the fault and footwall as well as the center of the fault, while the peak minimum principal stresses are mainly concentrated at the vault of the tunnel at the fault interfaces. The maximum and minimum principal stresses in the tunnel are concentrated at the

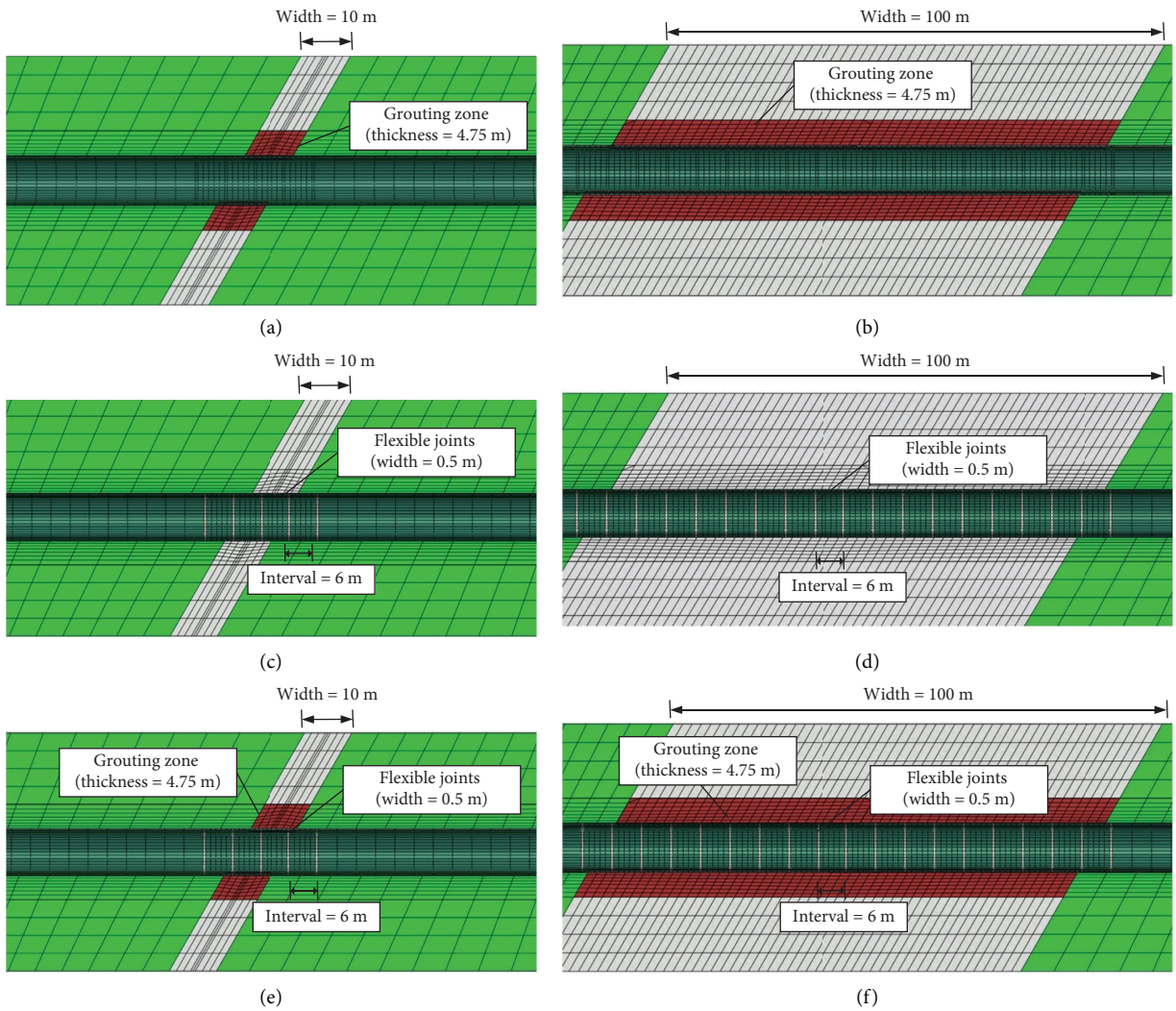

Figure 6: Installation of different aseismic measures: (a) 10 m fault with grouting; (b) 100 m fault with grouting; (c) 10 m fault with flexible joints; (d) 100 m fault with flexible joints; (e) 10 m fault with grouting and flexible joints; (f) 100 m fault with grouting and flexible joints.

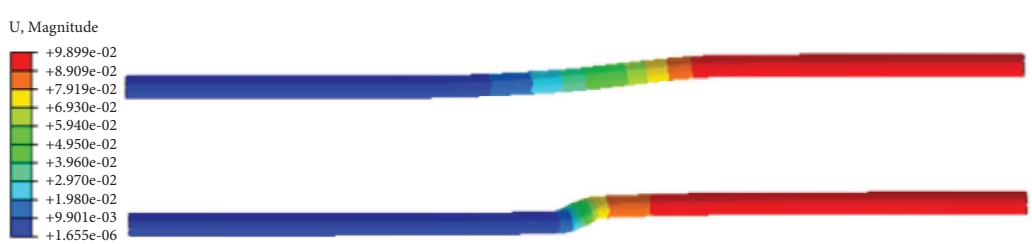

Figure 7: Diagram of tunnel deformation.

junctions of the tunnel and flexible joints when the flexible joints are installed.

In the synthetic wave case, grouting reduces the maximum principal stress to 35.2 MPa and the minimum principal stress to 25.8 MPa; the flexible joint increases the maximum principal stress to 56.6 MPa and the minimum principal stress to 54.6 MPa. For the model with both aseismic measures installed, the maximum principal stress in the tunnel is reduced to 42.3 MPa and the minimum principal stress is reduced to 31.9 MPa. In the Wenchuan wave case, grouting reduces the maximum principal stress to 26.1 MPa and the minimum principal stress to 28.4 MPa; flexible joints increase the maximum principal stress to 51.3 MPa and the minimum principal stress to 55.4 MPa; for the model with both aseismic measures installed, the maximum principal stress is reduced to 32.7 MPa and the

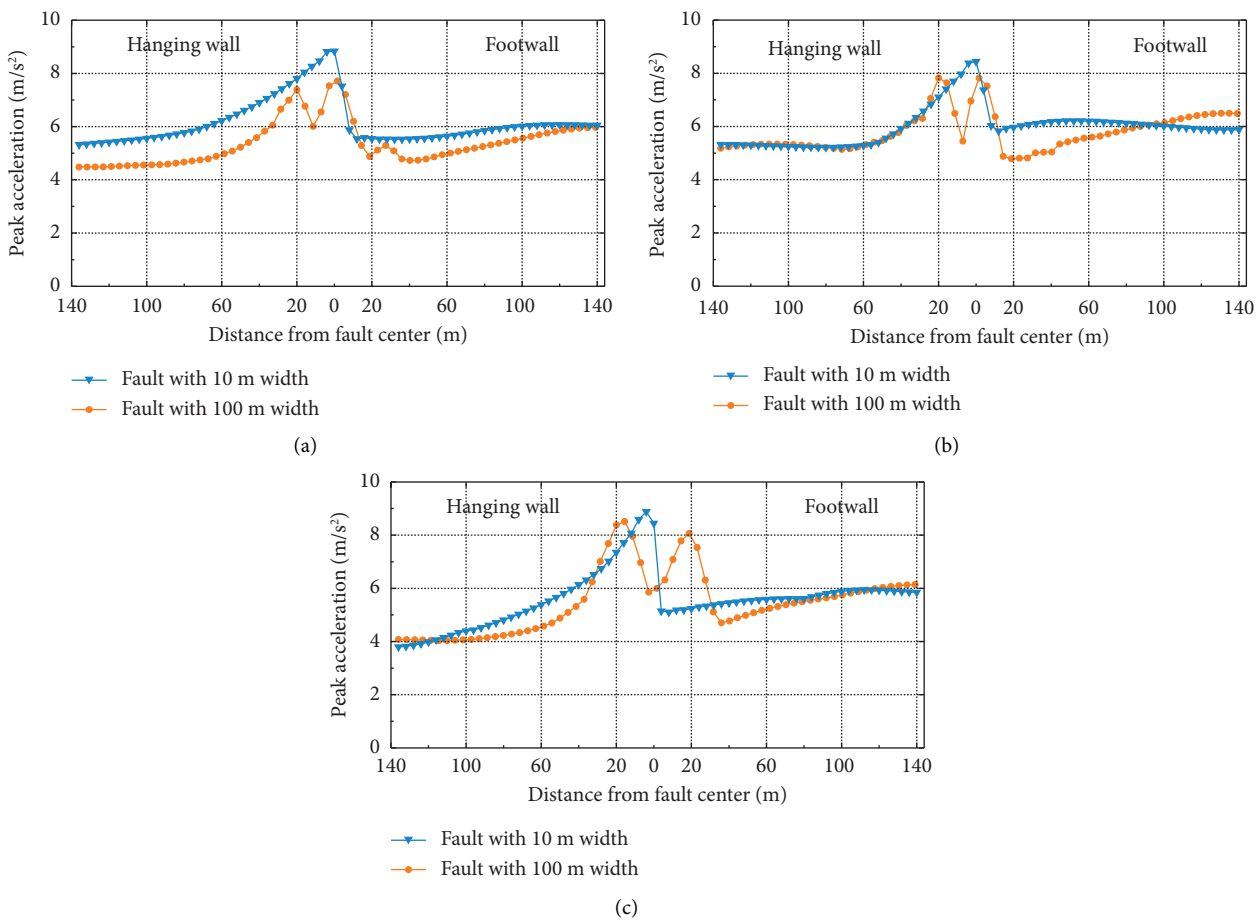

Figure 8: Peak acceleration of tunnels with different fault widths: (a) synthetic wave; (b) Wenchuan wave; (c) Kobe wave.

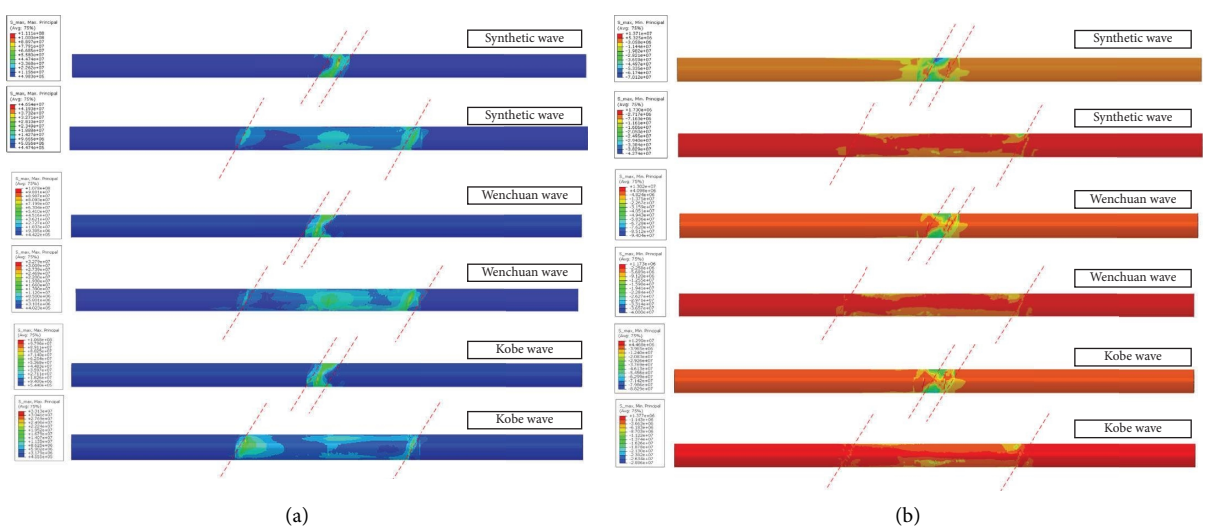

Figure 9: Principal stress contour of tunnels crossing different widths of faults: (a) maximum principal stress and (b) minimum principal stress.

minimum principal stress is increased to 49.9 MPa. In the Kobe wave case, grouting reduces the maximum principal stress to 23.3 MPa and the minimum principal stress to 25.2 MPa; flexible joints increase the maximum principal stress to 43.1 MPa and the minimum principal stress to 35.6 MPa; for the model with both aseismic measures

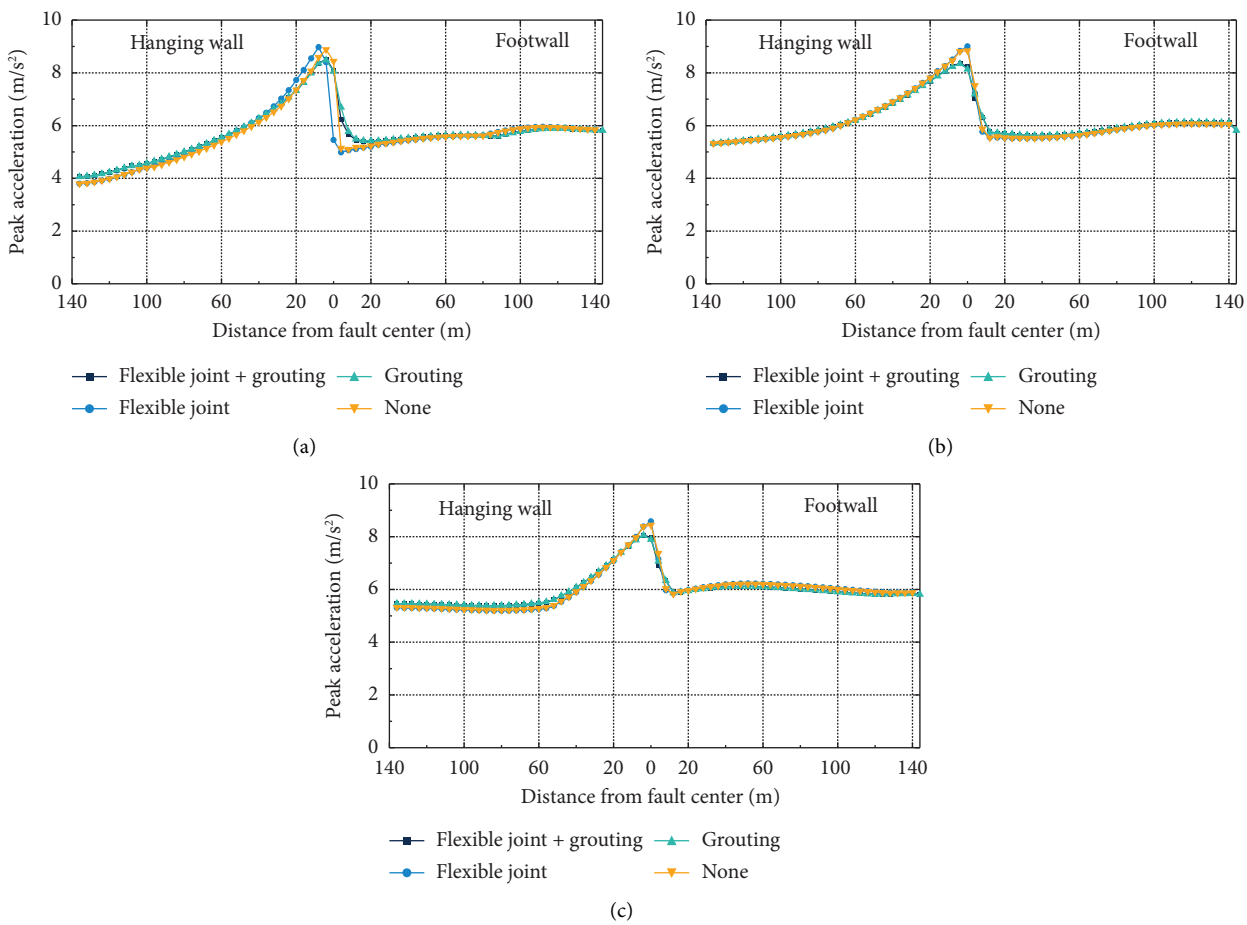

Figure 10: Peak acceleration of tunnels with different aseismic measures in a 10 m fault: (a) synthetic wave; (b) Wenchuan wave; (c) Kobe wave.

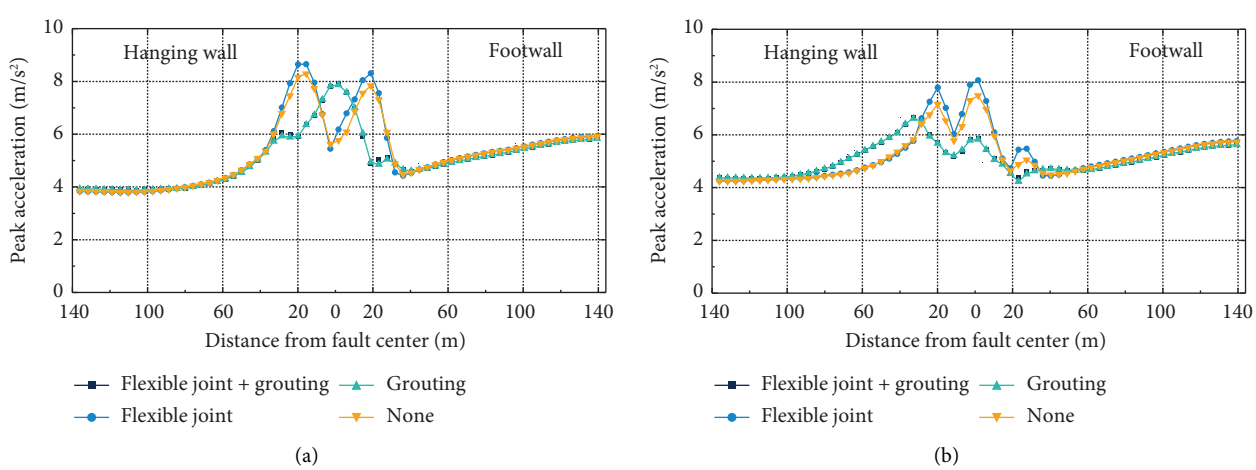

Figure 11: Continued.

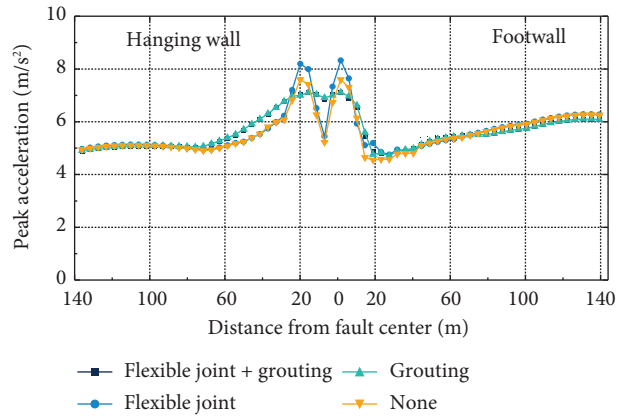

(c)

Figure 11: Peak acceleration of tunnels with different aseismic measures in a 100 m fault: (a) synthetic wave; (b) Wenchuan wave; (c) Kobe wave.

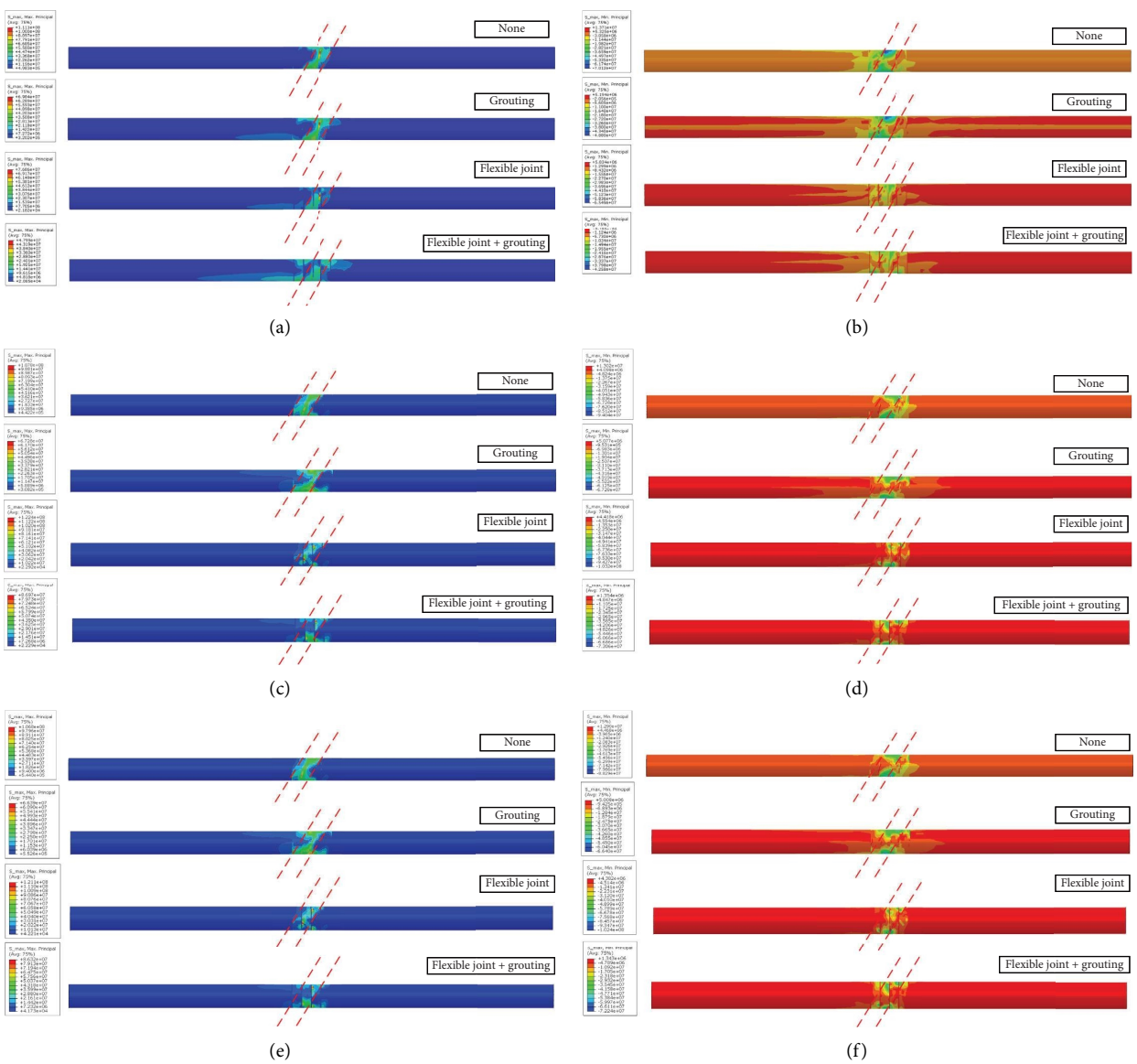

Figure 12: Principal stress of tunnels with different aseismic measures in a 10 m fault: (a) maximum principal stress in the synthetic wave case; (b) minimum principal stress in the synthetic wave case; (c) maximum principal stress in the Wenchuan wave case; (d) minimum principal stress in the Wenchuan wave case; (e) maximum principal stress in the Kobe wave case; (f) minimum principal stress in the Kobe wave case.

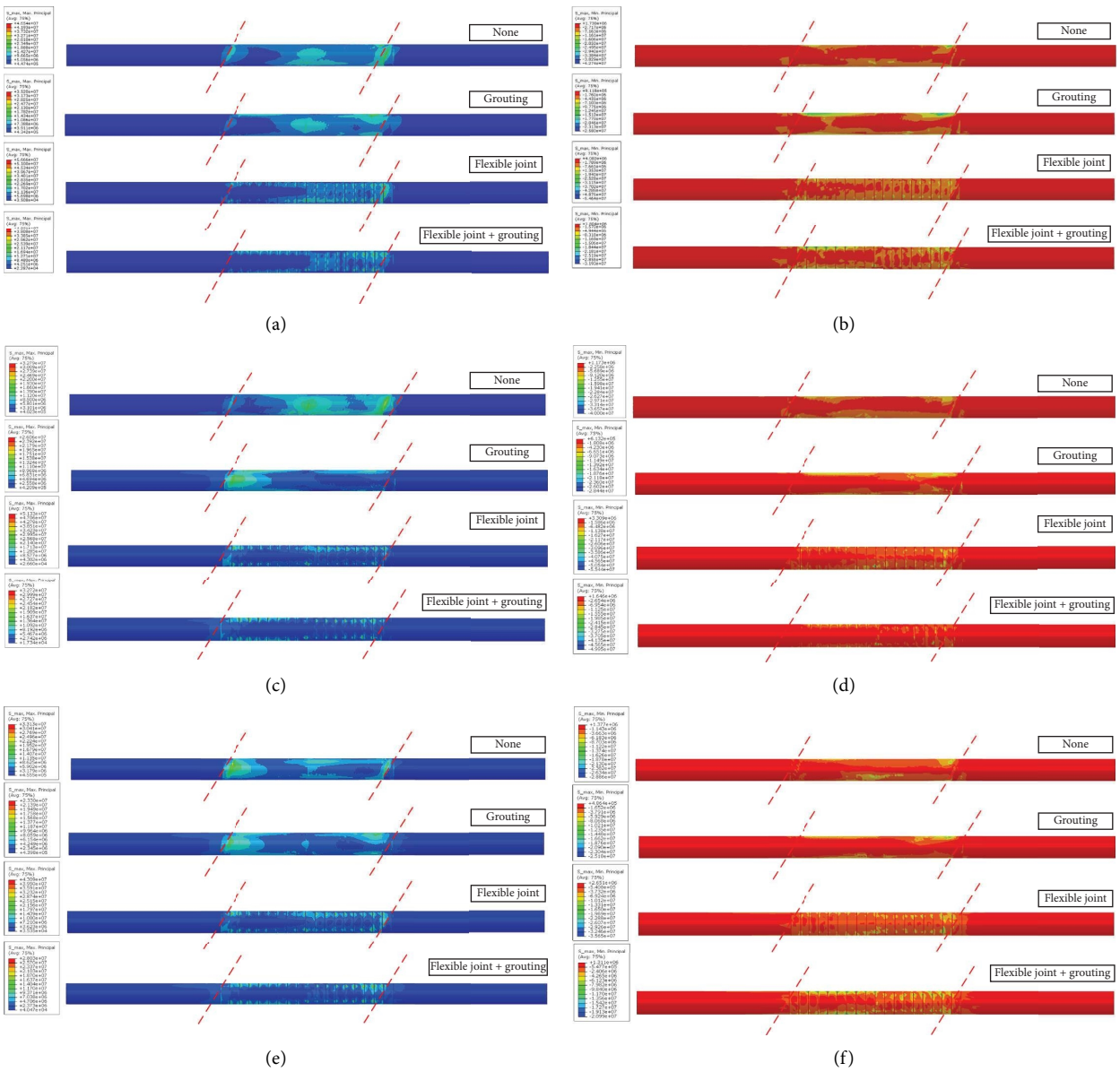

Figure 13: Principal stress of tunnels with different aseismic measures in a 100 m fault: (a) maximum principal stress in the synthetic wave case; (b) minimum principal stress in the synthetic wave case; (c) maximum principal stress in the Wenchuan wave case; (d) minimum principal stress in the Wenchuan wave case; (e) maximum principal stress in the Kobe wave case; (f) minimum principal stress in the Kobe wave case.

installed, the maximum principal stress is reduced to 28.0 MPa and the minimum principal stress is reduced to 21.0 MPa.

The peak principal stresses of the tunnel-crossing different fault widths are summarized in Table 3. It can be found that grouting can significantly reduce the tunnel response and has the best aseismic effect. Flexible joints reduce the longitudinal stiffness of the tunnel, which will increase the seismic response in earthquakes. Considering the feasibility of postearthquake restoration, the installation of both two aseismic measures can achieve both damping effects and economic benefits.

Table 3: Principal stress of tunnels with different aseismic measure.

Fault width	Case	Aseismic measure	Maximum principal stress (MPa)	Minimum principal stress (MPa)
10 m fault	Synthetic wave	None	111.1	70.1
		Flexible joint	76.9 (−30.8%)	65.5 (−6.6%)
		Grouting	69.8 (−37.2%)	48.8 (−30.4%)
		Flexible joint + grouting	48.0 (−56.8%)	42.6 (−39.2%)
	Wenchuan wave	None	107.8	94.0
		Flexible joint	122.2 (+13.3%)	103.2 (+9.8%)
		Grouting	67.3 (−37.6%)	67.3 (−28.4%)
		Flexible joint + grouting	86.9 (−19.4%)	73.1 (−22.2%)
	Kobe wave	None	106.8	88.3
		Flexible joint	121.1 (+13.4%)	102.4 (+15.9%)
		Grouting	66.4 (−37.8%)	66.4 (−24.8%)
		Flexible joint + grouting	86.3 (−19.2%)	72.2 (−18.2%)
100 m fault	Synthetic wave	None	46.5	42.7
		Flexible joint	56.6 (+21.7%)	54.6 (+27.9%)
		Grouting	35.2 (−24.3%)	25.8 (−39.6%)
		Flexible joint + grouting	42.3 (−9.0%)	31.9 (−25.3%)
	Wenchuan wave	None	32.8	40.0
		Flexible joint	51.3 (+56.4%)	55.4 (+38.5%)
		Grouting	26.1 (−20.4%)	28.4 (−29.0%)
		Flexible joint + grouting	32.7 (−1%)	49.9 (+24.7%)
	Kobe wave	None	33.1	28.9
		Flexible joint	43.1 (+30.2%)	35.6 (+23.2%)
		Grouting	23.3 (−29.6%)	25.2 (−12.8%)
		Flexible joint + grouting	28.0 (−15.4%)	20.9 (−27.7%)

4. Conclusions

In this paper, three-dimensional numerical models of tunnels crossing secondary faults are established and the seismic response of the fault-crossing tunnel under the combined action of ground motions and permanent fault dislocation of the fault is investigated. The aseismic effects of different aseismic measures are discussed. The following conclusions are obtained:

(1) For the model with a fault width of 100 m, peak tunnel acceleration has two peaks near the interfaces of the fault due to the reflection of seismic waves at the fault interfaces. While for the model with a fault width of 10 m, the two acceleration peaks overlap, making the peak tunnel acceleration within the fault exceed the peak tunnel acceleration within the fault with a width of 100 m.

(2) Since the permanent displacement of the fault will cause greater relative deformation of the tunnel within the fault when the fault width is narrow, the peak stress of the tunnel within the fault with a width of 10 m is much larger than that of the tunnel within the fault with a width of 100 m.

(3) For the model with a fault width of 10 m, setting different aseismic measures will not change the acceleration distribution pattern of the tunnel during earthquakes. For the model with a 100 m fault, the installation of grouting will reduce the larger acceleration response near the fault interfaces and small acceleration response in the center of the fault. Regardless of the fault width, the installation of flexible joints will slightly increase the acceleration response of the tunnel within the fault.

(4) For fault-crossing tunnels, grouting can significantly reduce the seismic response of tunnels. In some cases, the installation of flexible joints might increase the seismic response of tunnels. This is because installing flexible joints will reduce the longitudinal stiffness and integrity of the tunnel, which will increase the deformation of the tunnel during earthquakes and thus increase the stresses of the tunnel.

(5) Considering the feasibility of postearthquake restoration, the installation of both two aseismic measures can achieve both damping effects and economic benefits.

Data Availability

The data were attached in the figures.

Conflicts of Interest

The authors declare that they have no conflicts of interests.

Acknowledgments

This study was supported by the National Natural Science Foundation of China (41672289 and 51778487).

References

[1] Y. M. A. Hashash, J. J. Hook, B. Schmidt, and J. I-Chiang Yao, "Seismic design and analysis of underground structures,"

Tunnelling and Underground Space Technology, vol. 16, no. 4, pp. 247–293, 2001.

[2] Y. Shen, B. Gao, X. Yang, and S. Tao, "Seismic damage mechanism and dynamic deformation characteristic analysis of mountain tunnel after Wenchuan earthquake," *Engineering Geology*, vol. 180, pp. 85–98, 2014.

[3] H. Yu, J. Chen, Y. Yuan, and X. Zhao, "Seismic damage of mountain tunnels during the 5.12 Wenchuan earthquake," *Journal of Mountain Science*, vol. 13, no. 11, pp. 1958–1972, 2016b.

[4] X. Zhang, Y. Jiang, and S. Sugimoto, "Seismic damage assessment of mountain tunnel: a case study on the Tawarayama tunnel due to the 2016 Kumamoto Earthquake," *Tunnelling and Underground Space Technology*, vol. 71, pp. 138–148, 2018.

[5] Z. Chen, C. Shi, T. Li, and Y. Yuan, "Damage characteristics and influence factors of mountain tunnels under strong earthquakes," *Natural Hazards*, vol. 61, no. 2, pp. 387–401, 2012.

[6] W. L. Wang, T. T. Wang, J. J. Su, C. H. Lin, C. R. Seng, and T. H. Huang, "Assessment of damage in mountain tunnels due to the Taiwan Chi-Chi Earthquake," *Tunnelling and Underground Space Technology*, vol. 16, no. 3, pp. 133–150, 2001.

[7] H. Yu, J. Chen, A. Bobet, and Y. Yuan, "Damage observation and assessment of the Longxi tunnel during the Wenchuan earthquake," *Tunnelling and Underground Space Technology*, vol. 54, pp. 102–116, 2016a.

[8] M. H. Baziar, A. Nabizadeh, C. Jung Lee, and W. Yi Hung, "Centrifuge modeling of interaction between reverse faulting and tunnel," *Soil Dynamics and Earthquake Engineering*, vol. 65, pp. 151–164, 2014.

[9] L. Fan, J. Chen, P. ling et al., "Seismic response of tunnel under normal fault slips by shaking table test technique," *J. Cent. South Univ*.vol. 27, no. 4, pp. 1306–1319, 2020.

[10] X. Liu, X. Li, Y. Sang, and L. Lin, "Experimental study on normal fault rupture propagation in loose strata and its impact on mountain tunnels," *Tunnelling and Underground Space Technology*, vol. 49, pp. 417–425, 2015.

[11] Y. Ma, Q. Sheng, G. Zhang, and Z. Cui, "A 3D discrete-continuum coupling approach for investigating the deformation and failure mechanism of tunnels across an active fault: a case study of xianglushan tunnel," *Applied Sciences*, vol. 9, no. 11, p. 2318, 2019.

[12] X. Wang, Q. Xiong, H. Zhou, J. Chen, and M. Xiao, "Three-dimensional (3D) dynamic finite element modeling of the effects of a geological fault on the seismic response of underground caverns," *Tunnelling and Underground Space Technology*, vol. 96, Article ID 103210, 2020.

[13] Z. Yang, H. Lan, Y. Zhang, X. Gao, and L. Li, "Nonlinear dynamic failure process of tunnel-fault system in response to strong seismic event," *Journal of Asian Earth Sciences*, vol. 64, pp. 125–135, 2013.

[14] Z. Zhong, Z. Wang, M. Zhao, and X. Du, "Structural damage assessment of mountain tunnels in fault fracture zone subjected to multiple strike-slip fault movement," *Tunnelling and Underground Space Technology*, vol. 104, Article ID 103527, 2020.

[15] H. Jiao, X. Du, M. Zhao, J. Huang, X. Zhao, and W. Ouyang, "Nonlinear seismic response of rock tunnels crossing inactive fault under obliquely incident seismic P waves," *Journal of Earth Sciences*, vol. 32, no. 5, pp. 1174–1189, 2021.

[16] J. Huang, M. Zhao, and X. Du, "Non-linear seismic responses of tunnels within normal fault ground under obliquely incident P waves," *Tunnelling and Underground Space Technology*, vol. 61, pp. 26–39, 2017.

[17] Z. Liu, J. Liu, Q. Pei, H. Yu, C. Li, and C. Wu, "Seismic response of tunnel near fault fracture zone under incident SV waves," *Underground Space*, vol. 6, pp. 695–708, 2021.

[18] A. R. Shahidi and M. Vafaeian, "Analysis of longitudinal profile of the tunnels in the active faulted zone and designing the flexible lining (for Koohrang-III tunnel)," *Tunnelling and Underground Space Technology*, vol. 20, no. 3, pp. 213–221, 2005.

[19] Y. S. Shen, Z. Z. Wang, J. Yu, X. Zhang, and B. Gao, "Shaking table test on flexible joints of mountain tunnels passing through normal fault," *Tunnelling and Underground Space Technology*, vol. 98, Article ID 103299, 2020.

[20] Z. Chen, S. Liang, H. Shen, and C. He, "Dynamic centrifuge tests on effects of isolation layer and cross-section dimensions on shield tunnels," *Soil Dynamics and Earthquake Engineering*, vol. 109, pp. 173–187, 2018.

[21] Z. Z. Wang, Y. J. Jiang, and C. A. Zhu, "Seismic energy response and damage evolution of tunnel lining structures," *European Journal of Environmental and Civil Engineering*, vol. 23, no. 6, pp. 758–770, 2019.

[22] C. L. Xin, Z. Z. Wang, J. M. Zhou, and B. Gao, "Shaking table tests on seismic behavior of polypropylene fiber reinforced concrete tunnel lining," *Tunnelling and Underground Space Technology*, vol. 88, pp. 1–15, 2019.

[23] X. Zhao, R. Li, Y. Yuan, H. Yu, M. Zhao, and J. Huang, "Shaking table tests on fault-crossing tunnels and aseismic effect of grouting," *Tunnelling and Underground Space Technology*, vol. 125, Article ID 104511, 2022.

[24] B. Duan, "Inelastic response of compliant fault zones to nearby earthquakes," *Geophysical Research Letters*, vol. 37, no. 16, pp. 2–6, 2010.

[25] W. A. Chao, Y. M. Wu, and L. Zhao, "An automatic scheme for baseline correction of strong-motion records in coseismic deformation determination," *Journal of Seismology*, vol. 14, no. 3, pp. 495–504, 2010.

[26] R. Li, Y. Yuan, and X. Zhao, "Seismic response of tunnel across inactive fault: numerical analysis," *IOP Conference Series: Earth and Environmental Science*, vol. 861, no. 5, p. 052031, 2021.